

Article

Determination of Optic Axes by Corneal Topography among Italian, Brazilian, and Chinese Populations

Bernardo T. Lopes^{1,2,*}, Ashkan Eliasy¹, Mohamed Elhalwagy³, Riccardo Vinciguerra⁴, Fangjun Bao^{5,6}, Paolo Vinciguerra^{7,8}, Renato Ambrósio Jr.^{2,9}, Ahmed Elsheikh^{1,10,11} and Ahmed Abass¹

¹ School of Engineering, University of Liverpool, Liverpool L69 3GH, UK; eliasy@liverpool.ac.uk (A.E.); elsheikh@liverpool.ac.uk (A.E.); amfabass@liverpool.ac.uk (A.A.)

² Department of Ophthalmology, Federal University of São Paulo, São Paulo 04021, Brazil; dr.renatoambrosio@gmail.com

³ Institute of Translational Medicine, University of Liverpool, Liverpool L69 3BX, UK; M.Elhalwagy@liverpool.ac.uk

⁴ Humanitas San Pio X Hospital, 20159 Milano, Italy; vinciguerra.riccardo@gmail.com

⁵ School of Ophthalmology and Optometry and Eye Hospital, Wenzhou Medical University, Wenzhou 325035, China; bfjmd@126.com

⁶ Key Laboratory of Vision Science, Ministry of Health, Wenzhou 325035, China

⁷ Humanitas Clinical and Research Center—IRCCS Rozzano, 20089 Rozzano, Italy; paolo.vinciguerra@hunimed.eu

⁸ Department of Biomedical Sciences, Humanitas University, 20090 Pieve Emanuel, Italy

⁹ Department of Ophthalmology, Federal University the State of Rio de Janeiro (UNIRIO), Urca, Rio de Janeiro 22290, Brazil

¹⁰ Beijing Advanced Innovation Center for Biomedical Engineering, Beihang University, Beijing 100083, China

¹¹ NIHR Biomedical Research Centre for Ophthalmology, Moorfields Eye Hospital NHS Foundation Trust and UCL Institute of Ophthalmology, London EC1V 2PD, UK

* Correspondence: blopes@liverpool.ac.uk



Citation: Lopes, B.T.; Eliasy, A.; Elhalwagy, M.; Vinciguerra, R.; Bao, F.; Vinciguerra, P.; Ambrósio, R., Jr.; Elsheikh, A.; Abass, A. Determination of Optic Axes by Corneal Topography Among Italian, Brazilian, and Chinese Populations. *Photonics* **2021**, *8*, 61. <https://doi.org/10.3390/photonics8020061>

Academic editors:

Pablo Pérez-Merino, Andres Vasquez Quintero and Jos J. Rozema

Received: 18 December 2020

Accepted: 11 February 2021

Published: 23 February 2021

Publisher's Note: MDPI stays neutral with regard to jurisdictional claims in published maps and institutional affiliations.



Copyright: © 2021 by the authors. Licensee MDPI, Basel, Switzerland. This article is an open access article distributed under the terms and conditions of the Creative Commons Attribution (CC BY) license (<https://creativecommons.org/licenses/by/4.0/>).

Abstract: This study aims to describe a new universal method to identify the relative three-dimensional directions of visual, pupillary, and optical axes of the eye and the angles between them using topography elevation data. The method was validated in a large clinical cohort, and ethnical differences were recorded. Topography elevation data were collected from 1992 normal eyes of 966 healthy participants in Italy, Brazil, and China. The three main axes were defined as follows: optical axis (OA) was defined as the optimal path of light that passes through the ocular system without refraction. The pupillary axis (PA) line was defined using X and Y coordinates of the pupil centre with the chamber depth, in addition to the centre of a sphere fitted to the central 3 mm diameter of the cornea. The visual axis (VA) was taken by its best approximation, the coaxially sighted corneal light reflex. The alpha angle was measured between the VA and OA, and the kappa angle between the VA and PA. The average values of kappa and alpha angles were 3.41 ± 2.84 and 6.04 ± 2.43 in the Italian population, 2.6 ± 1.53 and 5.87 ± 2.3 in the Brazilian population, and 2.09 ± 1.22 and 3.85 ± 1.48 in the Chinese population.

Keywords: cornea; topography; optical axis; visual axis; pupillary axis; kappa angle; alpha angle

1. Introduction

As the human eye can be considered a non-aligned optical system [1,2], a number of theoretical and experimental axes exist which can be used to relate eye alignment and visual performance [3]. Among many other reasons for this non-alignment, the temporal location of the fovea and the relative nasal pupil deviation are of great importance. This leads to the presence of three main distinct axes: the visual, the optical, and the pupillary axes [4]. The visual axis is the line that passes through the fixation point, front nodal point, rear nodal point, and fovea of the eye [5], whereas the line that passes through the centre of the entrance pupil while normal to the corneal surface is defined as the pupillary axis. Finally,

the optical axis is the line that passes through the central corneal and stays normal to its surfaces [6]. In theory, it is comparable to the path of a light ray that enters and leaves the optical system of the eye along the same line [7]. The difference between the visual and the pupillary axes forms the kappa angle (κ), and between the visual and optical axes forms the alpha angle (α) [8].

It is known that the existence of these misalignments leads to optical aberrations that are balanced to improve the retinal image, either by different optical elements in the eye or by the incidence angle of the light rays [1,9]. However, the new customized laser refractive surgery and the implants of multifocal intraocular lenses (IOLs) disrupt this balance, and these new treatments need to be properly aligned in order to provide the perfect vision for patients [10,11].

The determination of these axes is challenging due to the absence of appropriate landmarks; therefore, some approximations must be done. The closest measurable point to the visual axis is the coaxially sighted corneal light reflex (CSCLR) [4,10]. However, the centre of the limbus is commonly used as a landmark to the optical axis, the limbus shape is not symmetrical, and its identification requires the acquisition of a sharp image of the anterior eye [12,13]. Additionally, the optical axis line meets the retina nasally below the fovea, missing its central sensitive zone [14], which makes it hard to be identified clinically [15]. Some new topographers and tomographers automatically measure the kappa angle (κ) [16–18]. However, just a few measure the alpha angle, the importance of which for IOL planning has been increasingly debated [19]. In brief, the optical centre of the IOL is generally positioned at the centre of the capsular bag, which is placed on the optical axis. The higher the alpha angle, the greater the chance of visual complaints in these patients [19]. The topographic exam is also affected by the physiological misalignment caused by the kappa angle. The corneal keratoconic pattern can be mimicked in patients with misalignments as small as 5° [20]. Therefore, some of these patients that could benefit from refractive surgery are excluded during preoperative screening by a misdiagnosis of ectasia susceptibility [21].

The aim of this study is to introduce a method that allows the identification of three main axes of the eye and the determination of the angles between them. This is done through accurate and systematic procedures that can be applied to all topography machines. This method was validated by clinical data from the continents of South America, Europe, and Asia, where the variations between the three main axes for three ethnicity groups were studied.

2. Materials and Methods

2.1. Clinical Data

The study involved the anonymised records of 343 Italian, 177 Brazilian, and 476 Chinese participants selected from referrals to the Vincieye Eye Clinic (Milan, Italy), Instituto de Olhos Renato Ambrósio (Rio de Janeiro, Brazil), and the Wenzhou Eye Hospital (Wenzhou, China). The clinical characteristics of participants' eyes as measured by the Pentacam HR software are listed in Table 1.

Clinical topography data have been collected from both eyes of normal participants from three populations in three different countries using the Pentacam HR (OCULUS Optikgeräte GmbH, Wetzlar, Germany). Participants from Italy, Brazil, and China with no history of ocular disease, trauma, or ocular surgery were selected. Those with intraocular pressure (IOP) higher than 21 mmHg as measured by the Goldmann Applanation Tonometer were excluded, along with those who wore soft contact lenses less than two weeks before measurement and those who wore rigid gas-permeable (RGP) contact lenses less than four weeks before measurements.

Raw Pentacam HR elevation data were used in this study, therefore, it was free of the effect of using any mathematical extrapolation techniques. Using the raw data in this study granted the absence of the effect of any smoothing algorithm that could be embedded in the Pentacam HR software. The raw elevation data were exported in a comma-separated

values (CSV) format and analysed using custom-built Matlab[®] (MathWorks, Natick, USA) codes written specifically for this study.

Table 1. Clinical data and characteristics of participants' eyes as measured by the Pentacam HR.

	Italian Participants		Brazilian Participants		Chinese Participants	
Participants (eyes)	347 (694)		181 (362)		500 (1000)	
Age in years; mean ± SD (min: max)	37.6 ± 13.5 (6: 106)		35.6 ± 15.8 (10: 87)		24.2 ± 5.7 (17: 48)	
Clinical features and angles	Mean ± SD	Min : Max	Mean ± SD	Min : Max	Mean ± SD	Min : Max
Minimum corneal thickness (µm)	531 ± 420	404:706	550 ± 33	492:660	535 ± 290	453:620
Flat curvature in the central 3 mm zone K1 (D)	42.3 ± 1.9	36.6:47.8	42.6 ± 1.4	39.4:46.6	42.8 ± 1.4	38.2:48.1
Steep curvature in the central 3 mm zone K2 (D)	44.3 ± 2.9	37.1:51.4	43.8 ± 1.5	40.3:47.9	43.9 ± 1.6	38.6:49.5
Index of Bad D	1.2 ± 0.8	−0.7:3.0	0.4 ± 0.5	−0.9:1.4	1.0 ± 0.6	−0.8:3.0
Kappa angle (κ)	3.33 ± 1.97	0.09:12.99	2.60 ± 1.52	0.27:10.26	2.09 ± 1.23	0.07:8.68
Alpha angle (α)	5.60 ± 2.48	0.57:18.77	5.38 ± 1.74	0.57:11.22	4.34 ± 1.30	0.81:8.45

SD: Standard deviation. D: Dioptres. Bad D: final index of belin ambrosio display.

2.2. Determination of the Optical Axis

To determine the corneal optical axis, as it is defined in the literature as the path of light that goes through the ocular system without refraction, a light ray tracing algorithm was coded in MATLAB software, and then validated graphically via AutoCAD software.

The light ray tracing performance was obtained by simulating parallel light rays directed towards the cornea and refracted through the anterior and posterior surfaces according to Snell's law [22,23] (Figure 1). The incidence angle for each ray in the air, \varnothing_{air} , was determined as the angle between the ray and normal vector to the corneal surface at the point of incidence (Figure 1a). The direction of the refracted ray as it passed through the corneal depth, $\varnothing_{cornea_anterior}$, was calculated by Equation (1), where the refractive indices of air, n_{air} , cornea, n_{cornea} , and aqueous, $n_{aqueous}$ were set to 1.0, 1.376, and 1.336, respectively, following Gullstrand's relaxed eye model [22,24].

$$\varnothing_{cornea_anterior} = \sin^{-1} \left(\frac{n_{air}}{n_{cornea}} \sin \varnothing_{air} \right) \quad (1)$$

Each light ray refracted by the cornea's anterior surface was then used as an incident ray on the posterior surface with an incidence angle $\varnothing_{cornea_posterior}$, before being refracted again when it passed through the posterior surface and then left with angle $n_{aqueous}$ through the aqueous (Equation (2)).

$$\varnothing_{aqueous} = \sin^{-1} \left(\frac{n_{cornea}}{n_{aqueous}} \sin \varnothing_{cornea_posterior} \right) \quad (2)$$

The next step was to locate the point of intersection between the refracted light ray and the corneal longitudinal axis. From this point, the focal length f of each light ray could be calculated as the distance from this point to the corneal apex. With f determined, the optical power could be calculated as [25]:

$$P = \frac{n_{aqueous}}{f} \quad (3)$$

In this analysis, it was noted that not all rays intersect the corneal axis due to the existence of spherical aberration. In these cases, the closest points on the corneal visual axis to the refracted light rays were taken as the focal points [26].

Since the optical axis is defined as when a straight light ray enters and leaves an optical system along the same line [7] without refraction, such that the line may be located by two points on the corneal anterior and posterior surfaces. When a light ray penetrates the corneal surfaces without refraction, the focal length of this line will be infinity, and its power will tend towards zero according to Equation (3).

Corneal topography data of each eye were rotated in three dimensions in an optimisation loop, while the simulated light rays were kept parallel to themselves towards the cornea.

The optimisation looping procedure was set to end when one of the simulated light rays recorded an infinite focal length and, as a result, zero optical power. This process was carried out by the Levenberg–Marquardt nonlinear least squares algorithm (LMA) [27,28] via the MATLAB Optimisation Toolbox. The LMA algorithm was set to stop the optimisation process when the smallest ray's optical power was below 1×10^{-20} . The optimisation strategy adopted was the rotation of the corneal surfaces around y axes and x axes by angles α_x and α_y , respectively, in order to minimise the optical power of a central light ray, and then select it as the optimal optical axis. The optimisation process for each eye's topography produced the optimal values of the rotation angles α_x and α_y , which can be used to locate the optimal location of the eye's optical axis. The rotation was achieved by the following three rotation matrices [29], where α_z was set to zero:

$$R_x(\alpha_x) = \begin{bmatrix} 1 & 0 & 0 \\ 0 & \cos \alpha_x & -\sin \alpha_x \\ 0 & \sin \alpha_x & \cos \alpha_x \end{bmatrix} \quad (4)$$

$$R_y(\alpha_y) = \begin{bmatrix} \cos \alpha_y & 0 & \sin \alpha_y \\ 0 & 1 & 0 \\ -\sin \alpha_y & 0 & \cos \alpha_y \end{bmatrix} \quad (5)$$

$$R_z(\alpha_z) = \begin{bmatrix} \cos \alpha_z & -\sin \alpha_z & 0 \\ \sin \alpha_z & \cos \alpha_z & 0 \\ 0 & 0 & 1 \end{bmatrix} = \begin{bmatrix} 1 & 0 & 0 \\ 0 & 1 & 0 \\ 0 & 0 & 1 \end{bmatrix} \quad (6)$$

Following the elemental rotation rule, the rotated coordinates of the corneal surface X_r , Y_r , and Z_r were calculated as

$$\begin{bmatrix} x_{r1} & x_{r2} & x_{r3} & \dots & x_{rn} \\ y_{r1} & y_{r2} & y_{r3} & \dots & y_{rn} \\ z_{r1} & z_{r2} & z_{r3} & \dots & z_{rn} \end{bmatrix} = [R_x(\alpha_x) * R_y(\alpha_y) * R_z(\alpha_z)] * \begin{bmatrix} x_1 & x_2 & x_3 & \dots & x_n \\ y_1 & y_2 & y_3 & \dots & y_n \\ z_1 & z_2 & z_3 & \dots & z_n \end{bmatrix} \quad (7)$$

Then, the light ray tracing process resumed in the optimisation loop after each rotation. In total, 1992 Pentacam comma-separated values (CSV) input data files were managed with an average processing time of 1.5 h per file in a four-core central processing unit (CPU). The 2988 h of optimisation time were split among eight computers that worked in parallel for 16 days.

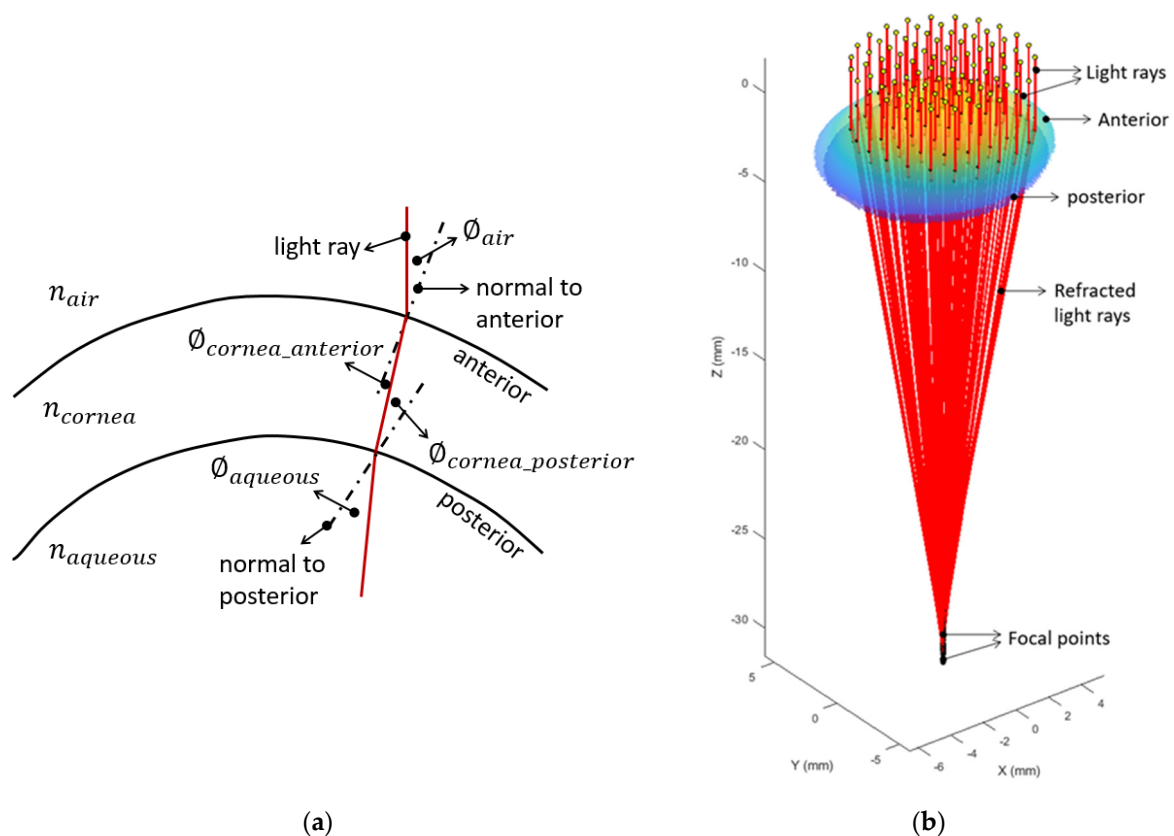


Figure 1. Light ray tracing method. (a) Single light ray tracing, (b) full resolution light ray tracing.

2.3. Determination of the Pupillary Axis

Following the Cartesian coordinate system, entrance pupil XY centre coordinate data were extracted from the Pentacam elevation CSV files automatically by a custom-built MATLAB code. In order to locate the centre of the entrance pupil back to its natural position, the Pentacam chamber depth value was extracted by the MATLAB code. This value was used to shift the centre of the entrance pupil Z coordinates back to its natural position. The point located by entrance pupil centre XY data and the chamber depth were considered as the first points in the entrance pupil axis. The second point in the entrance pupil axis was calculated by fitting a sphere to the central 3 mm diameter of the cornea, finding the centre of this sphere, and then drawing a line passing through the centre of the entrance pupil and the centre of this fitted sphere. This line represented the pupillary axis, coloured as blue in Figure 2.

2.4. Determination of the Visual Axis

During the scanning of the eye with the Pentacam HR Scheimpflug tomographer, the eye became oriented in such a way that the coaxially sighted corneal light reflex (CSCLR), which has been demonstrated in theoretical analysis and clinical studies to be the best approximation of the visual axis [10,30], aligns with the tomographer's axis; therefore, the visual axis was taken as the axis of the rotating Pentacam Scheimpflug camera. The intersection of the visual axis with both the corneal surface and the entrance pupil plan was determined as shown in Figure 2, where the visual axis is coloured in green.

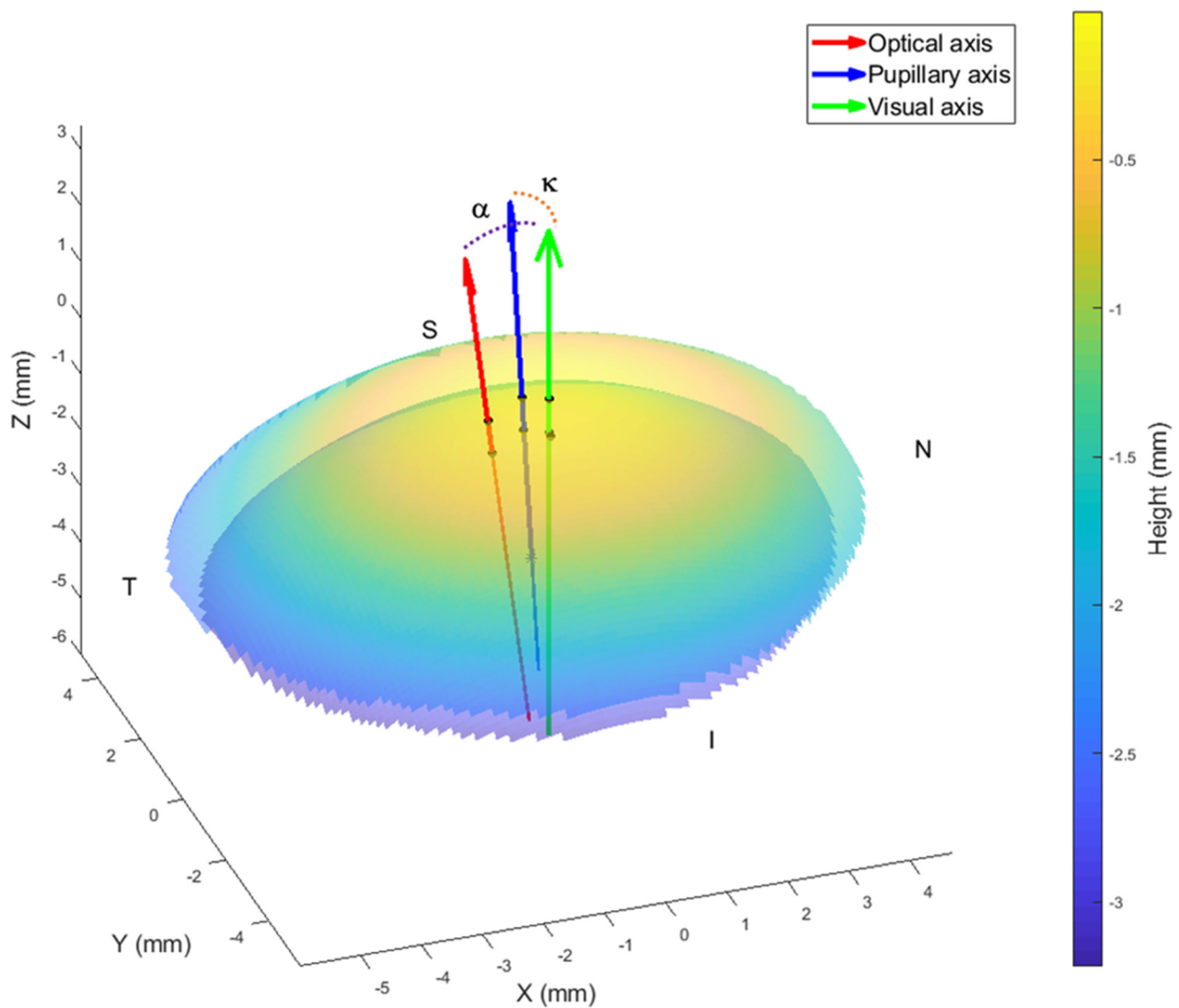


Figure 2. Three-dimensional positions of the visual, pupillary, and optical axes with the corresponding alpha (α) and kappa (κ) angles in the right eye of an Italian participant. N, T, S, and I stand for the nasal, temporal, superior, and inferior sides of the cornea, respectively.

2.5. Statistical Analysis

Statistical analysis was performed using Matlab Statistics and Machine Learning Toolbox (MathWorks, Natick, MA, USA). The null hypothesis probability (p) at a 95% confidence level was calculated. Paired and unpaired sample t -tests were used to investigate the significance between samples of data sets to check whether the results represented an independent record. The probability p is an element of the period $[0, 1]$, where values of p higher than 0.05 indicated the validity of the null hypothesis [31].

3. Results

A total of 2056 eyes from 1028 patients from three different continents were included in this study. The age distribution was different among the groups ($p < 0.0001$). The oldest population was from Italy, 37.6 ± 13.5 (6–106), followed by Brazil, 35.6 ± 15.8 (10–87) and China 24.2 ± 5.7 (17–48). Table 1 summarizes the distribution of corneal characteristics among the populations.

The distribution of kappa and alpha angles is summarized in Table 2. Regarding the laterality of kappa and alpha angles, the Chinese population presented higher values in the

left eye, while the Italian and Brazilian populations presented higher values in the right eye. Higher differences between the eyes were found in the kappa angle. The only statistically significant difference in terms of laterality was present in the kappa angle distribution of the Italian population ($p < 0.0001$).

Since the Chinese population was significantly younger, two age groups were defined (less than 20 years and from 20 to 40 years) in order to compare all populations. No statistically significant difference was found between the age groups in the same population. However, there was a slightly decreasing trend in the alpha angle with age for all populations, and a slightly increasing trend in the kappa angle for the Brazilian and Chinese populations, while the Italian group presented the opposite behaviour.

Table 2. The kappa (κ) and alpha (α) angle distribution between eyes and with age.

Eye side	Italian Participants			Brazilian Participants			Chinese Participants		
	Right eye Mean \pm SD Min:Max	Left eye Mean \pm SD Min:Max	<i>p</i> -value	Right eye Mean \pm SD Min:Max	Left eye Mean \pm SD Min:Max	<i>p</i> -value	Right eye Mean \pm SD Min:Max	Left eye Mean \pm SD Min:Max	<i>p</i> -value
κ (degree)	3.80 \pm 2.04 0.36:9.58	2.85 \pm 1.76 0.09:12.99	< 0.001	2.70 \pm 1.41 0.34:7.31	2.49 \pm 1.62 0.27:10.27	0.087	2.03 \pm 1.24 0.07:8.17	2.15 \pm 1.22 0.12:8.68	0.022
α (degree)	5.64 \pm 2.30 0.57:14.92	5.55 \pm 2.65 0.57:18.77	0.518	5.40 \pm 1.74 1.03:11.22	5.37 \pm 1.75 0.57:11.18	0.646	4.31 \pm 1.28 0.81:8.45	4.37 \pm 1.31 0.85:8.20	0.284
Age Strata	< 20 years (n = 38)	20–40 years (n = 356)	<i>p</i> -value	< 20 years (n = 28)	20–40 years (n = 230)	<i>p</i> -value	< 20 years (n = 328)	20–40 years (n = 652)	<i>p</i> -value
	Mean \pm SD Min:Max	Mean \pm SD Min:Max		Mean \pm SD Min:Max	Mean \pm SD Min:Max		Mean \pm SD Min:Max	Mean \pm SD Min:Max	
κ (degree)	3.58 \pm 1.93 0.94:7.95	3.31 \pm 1.97 0.09:12.99	0.409	2.22 \pm 1.53 0.32:7.55	2.63 \pm 1.52 0.27:10.27	0.391	2.00 \pm 1.16 0.13:7.81	2.14 \pm 1.26 0.07:8.68	0.501
α (degree)	5.95 \pm 2.72 1.92:14.92	5.57 \pm 2.46 0.57:18.77	0.418	5.67 \pm 1.84 2.23:9.39	5.36 \pm 1.73 0.57:11.22	0.187	4.38 \pm 1.25 0.81:7.81	4.32 \pm 1.32 0.81:8.45	0.085

4. Discussion

This study introduced a novel method to determine the main axes of the eye, which can be applied to topographical elevation data from Scheimpflug-based systems. We also evaluated the distribution of the alpha and kappa angles in three different ethnic groups, which may play an important role in certain refractive procedures [10]. These misalignments between the axes of the eye are relevant to ophthalmic surgical procedures and diagnosis. They are increasingly used in clinical practice, but are only available in some commercial devices [16–18], especially the alpha angle [19].

When taking a topographic measurement, the patient aligns their line of sight with the optic axis of the device. Since the fovea is shifted temporally, the centre of the map will be slightly nasal. Due to the aspherical shape of the cornea, the peripheral measures present bigger radii than those obtained near the central area [32]. The bigger the distance between the visual axis and the pupillary or the optic axis, the more distortions on the axial map will be produced. Hubbe and Foulks did repeated measurements in patients, fixating at points progressively further away from the visual axis. In some patients, a deviation of less than five degrees produced an asymmetric pattern that mimics keratoconus [20]. The correct determination of the main ocular axes is important to improve the diagnosis of corneal ectatic diseases.

In refractive surgery, higher kappa angle values are related to de-centred ablation and aggravation of visual symptoms [33]. Reinstein et al. demonstrated that high hyperopic corneal ablations presented similar results in patients with high and low kappa angles, supporting that the entrance pupil centre is not a good landmark for the centration of the procedure, and the evaluation of ocular axes is essential for a good surgical outcome [10].

The correct evaluation of the ocular axes is also fundamental in premium IOL implantation. Prakash et al. observed a positive correlation with visual symptoms after multifocal IOL implantation with preoperative kappa angle values [11]. The alpha angle should also be properly characterized, whereas the optical centre of the IOL relies on the centre of the capsular bag, which coincides with the optical axis. The higher the value of the alpha angle, the more de-centred the IOL will be. Roop proposed a new IOL design where the centre of the lens is nasally shifted, producing better optical outcomes experimentally [19].

Regarding the distribution, the kappa and alpha angles differed among the populations. The Chinese population presented the lowest values ($\alpha = 4.34 \pm 1.30^\circ$, $\kappa = 2.09 \pm 1.23^\circ$), followed by the Brazilian ($\alpha = 5.38 \pm 1.74^\circ$, $\kappa = 2.6 \pm 1.52^\circ$) and the Italian ($\alpha = 5.60 \pm 2.48^\circ$, $\kappa = 3.33 \pm 1.97^\circ$). The overall value of the kappa angle was lower than the ones obtained from different commercial devices reported previously in the literature [16,17,34–36]. However, the reported values of the kappa angle differ among different devices [16] and between the topographer and the Synoptophore [17], which exhibit lower values, such as the ones reported in this study.

The difference among the populations found in our study may rely on the different ethnic backgrounds, but also in the different age distribution of the populations, with the Chinese population presenting the younger participants. These results are aligned with the ones from Choi and Kim, who observed an increase in the kappa angle with age in a Korean population with a mean age of 58.4 years [34].

Gharaee et al. analysed a younger cohort of Iranians from 18 to 45 years. They found a decrease in the kappa angle with age in younger patients. Evaluating our results by two different strata of age, below 20 years and between 20 and 40 years, the trend of a decrease in the kappa angle value with increasing age, although not statistically significant, was observed in the Italian population, but was not observed in the Brazilian or the Chinese populations. Regarding the alpha angle, it presented a non-significant, mild decreasing trend with age in all three populations. This different distribution may be a consequence of different ethnic backgrounds.

Some differences were found between right and left eyes. Regarding the alpha angle, none of the studied populations presented a statistically significant difference between the eyes. The kappa angle was higher in the right eye among Italian and Brazilian participants, with statistical significance in the Italian population ($p < 0.001$ and 0.087 , respectively), and was significantly higher in the left eyes among the Chinese participants ($p = 0.022$). There are some conflicting results in the literature in relation to this subject. Basmak et al. reported higher values of the kappa angle in the left eye, while Gharaee et al. reported higher values of the kappa angle in the right eye [17,35]. Some hypotheses may be proposed to explain this difference, such as correlation to eye dominance and facial asymmetries or head posture, which may affect the distance from the eye to the topographer and the reference angles, but these were not evaluated in this study, and further investigations are needed to clarify this aspect.

5. Conclusions

In conclusion, we proposed and validated the consistency in a big cohort of clinical cases of a new universal method to evaluate the different positions of the ocular axes. Some variations with age and eye laterality were observed among the different groups. Some of the variances may be explained by the difference in the ethnic background of the groups. On average, the younger and the western populations studied were the ones that presented the higher values in both kappa and alpha angles. This information can help clinicians in preoperative screening.

Author Contributions: Conceptualization, A.A. and A.E. (Ahmed Elsheikh); methodology, A.A.; formal analysis, B.T.L. and A.E. (Ashkan Eliasy); data curation, R.V., P.V., R.A., and F.B.; writing—original draft preparation, B.T.L. and A.E. (Ashkan Eliasy); writing—review and editing, A.A., A.E. (Ahmed Elsheikh), M.E., R.V., P.V., R.A., and F.B.; supervision, A.A. All authors have read and agreed to the published version of the manuscript.

Funding: This research received no external funding.

Institutional Review Board Statement: Ethical review and approval were waived for this study, due to the use of fully anonymised secondary clinical data.

Conflicts of Interest: R.V., P.V., R.A., and A. Elshiekh are consultants for Oculus Optikgeräte GmbH, Wetzlar, Germany. The remaining authors declare no conflict of interest. The funder had no role in the design of the study; in the collection, analyses, or interpretation of data; in the writing of the manuscript, or in the decision to publish the results.

References

1. Berrio, E.; Tabernero, J.; Artal, P. Optical aberrations and alignment of the eye with age. *J. Vis.* **2010**, *10*. [[CrossRef](#)] [[PubMed](#)]
2. Keller, P.R.; Saarloos, P.P. Perspectives on corneal topography: A review of videokeratoscopy. *Clin. Exp. Optom.* **1997**, *80*, 18–30. [[CrossRef](#)]
3. Douthwaite, W.A.; Pardhan, S. Surface tilt measured with the EyeSys videokeratoscope: Influence on corneal asymmetry. *Investig. Ophthalmol. Vis. Sci.* **1998**, *39*, 1727–1735.
4. Pande, M.; Hillman, J.S. Optical zone centration in keratorefractive surgery. Entrance pupil center, visual axis, coaxially sighted corneal reflex, or geometric corneal center? *Ophthalmology* **1993**, *100*, 1230–1237. [[CrossRef](#)]
5. Harris, W.F. Nodes and nodal points and lines in eyes and other optical systems. *Ophthalmic Physiol. Opt.* **2010**, *30*, 24–42. [[CrossRef](#)]
6. Schwiegerling, J.T. Eye axes and their relevance to alignment of corneal refractive procedures. *J. Refract. Surg.* **2013**, *29*, 515–516. [[CrossRef](#)]
7. Arba Mosquera, S.; Verma, S.; McAlinden, C. Centration axis in refractive surgery. *Eye Vis.* **2015**, *2*, 4. [[CrossRef](#)]
8. Moshirfar, M.; Hoggan, R.N.; Muthappan, V. Angle Kappa and its importance in refractive surgery. *Oman J. Ophthalmol.* **2013**, *6*, 151–158. [[CrossRef](#)]
9. Espinosa, J.; Mas, D.; Kasprzak, H.T. Corneal primary aberrations compensation by oblique light incidence. *J. Biomed. Opt.* **2009**, *14*, 044003. [[CrossRef](#)]
10. Reinstein, D.Z.; Gobbe, M.; Archer, T.J. Coaxially sighted corneal light reflex versus entrance pupil center centration of moderate to high hyperopic corneal ablations in eyes with small and large angle kappa. *J. Refract. Surg.* **2013**, *29*, 518–525. [[CrossRef](#)] [[PubMed](#)]
11. Prakash, G.; Prakash, D.R.; Agarwal, A.; Kumar, D.A.; Agarwal, A.; Jacob, S. Predictive factor and kappa angle analysis for visual satisfactions in patients with multifocal IOL implantation. *Eye* **2011**, *25*, 1187–1193. [[CrossRef](#)] [[PubMed](#)]
12. Van Buskirk, E.M. The anatomy of the limbus. *Eye* **1989**, *3 Pt 2*, 101–108. [[CrossRef](#)] [[PubMed](#)]
13. Consejo, A.; Llorens-Quintana, C.; Radhakrishnan, H.; Iskander, D.R. Mean shape of the human limbus. *J. Cataract Refract. Surg.* **2017**, *43*, 667–672. [[CrossRef](#)]
14. Yang, Q.; Cho, K.-S.; Chen, H.; Yu, D.; Wang, W.-H.; Luo, G.; Pang, I.-H.; Guo, W.; Chen, N.F. Microbead-induced ocular hypertensive mouse model for screening and testing of aqueous production suppressants for glaucoma. *Investig. Ophthalmol. Vis. Sci.* **2012**, *53*, 3733–3741. [[CrossRef](#)]
15. Thibos, L.N.; Bradley, A.; Still, D.L.; Zhang, X.; Howarth, P.A. Theory and measurement of ocular chromatic aberration. *Vis. Res.* **1990**, *30*, 33–49. [[CrossRef](#)]
16. Dominguez-Vicent, A.; Monsalvez-Romin, D.; Perez-Vives, C.; Ferrer-Blasco, T.; Montes-Mico, R. Measurement of angle Kappa with Orbscan II and Galilei G4: Effect of accommodation. *Graefes Arch. Clin. Exp. Ophthalmol.* **2014**, *252*, 249–255. [[CrossRef](#)]
17. Basmak, H.; Sahin, A.; Yildirim, N.; Papakostas, T.D.; Kanellopoulos, A.J. Measurement of angle kappa with synoptophore and Orbscan II in a normal population. *J. Refract. Surg.* **2007**, *23*, 456–460. [[CrossRef](#)]
18. Qi, H.; Jiang, J.J.; Jiang, Y.M.; Wang, L.Q.; Huang, Y.F. Kappa angles in different positions in patients with myopia during LASIK. *Int. J. Ophthalmol.* **2016**, *9*, 585–589. [[CrossRef](#)]
19. Roop Roop, P. Optimizing optical outcomes of intraocular lens implantation by achieving centration on visual axis. *Indian J. Ophthalmol.* **2017**, *65*, 1425–1427. [[CrossRef](#)]
20. Hubbe, R.E.; Foulks, G.N. The effect of poor fixation on computer-assisted topographic corneal analysis. *Ophthalmology* **1994**, *101*, 1745–1748.
21. Doyle, S.J.; Hynes, E.; Naroo, S.; Shah, S. PRK in patients with a keratoconic topography picture. The concept of a physiological ‘displaced apex syndrome’. *Br. J. Ophthalmol.* **1996**, *80*, 25–28. [[CrossRef](#)]
22. Smit, G.; Atchison, D.A. *The eye and visual optical instruments*; Cambridge University Press: Cambridge, UK, 1970.
23. Smith, D.A.G. *Optics of the Human Eye*; Reed Educational and Professional Publishing Ltd.: Edinburgh, UK, 2000; 261p.
24. Vojnikovi, B.; Tamajo, E. Gullstrand’s Optical Schematic System of the Eye Modified by Vojnikovi & Tamajo. *Coll. Antropol.* **2013**, *37*, 41–45.
25. Wang, L.; Mahmoud, A.M.; Anderson, B.L.; Koch, D.D.; Roberts, C.J. Total corneal power estimation: Ray tracing method versus gaussian optics formula. *Investig. Ophthalmol. Vis. Sci.* **2011**, *52*, 1716–1722. [[CrossRef](#)]
26. Welford, W.T. *Aberrations of Optical Systems*; CRC Press: Boca Raton, FL, USA; Taylor & Francis: Abingdon, UK, 1986.

27. Guyon, F.; Riche, R.L. *Least Squares Parameter Estimation and the Levenberg-Marquardt Algorithm: Deterministic Analysis; Sensitivities and Numerical Experiments*; INSA de Rouen: Saint-Étienne-du-Rouvray, France, 1999.
28. Björck, A. *Numerical Methods for Least Squares Problems*. Philadelphia: Society for Industrial and Applied Mathematics. Available online: <https://doi.org/10.1137/1.9781611971484> (accessed on 15 February 2021).
29. Arvo, J. Fast Random Rotation Matrices. In *Graphics Gems III*; David, K., Ed.; Academic Press Professional, Inc.: Cambridge, MA, USA, 1992; pp. 117–120.
30. Mrochen, M.; Kaemmerer, M.; Mierdel, P.; Seiler, T. Increased higher-order optical aberrations after laser refractive surgery: A problem of subclinical decentration. *J. Cataract Refract. Surg.* **2001**, *27*, 362–369. [[CrossRef](#)]
31. Everitt, B.S.; Skrondal, A. *The Cambridge Dictionary of Statistics*, 4th ed.; Cambridge University Press: Cambridge, UK, 2010.
32. Chan, J.S.; Mandell, R.B.; Burger, D.S.; Fusaro, R.E. Accuracy of videokeratography for instantaneous radius in keratoconus. *Optom. Vis. Sci.* **1995**, *72*, 793–799. [[CrossRef](#)]
33. Park, C.Y.; Oh, S.Y.; Chuck, R.S. Measurement of angle kappa and centration in refractive surgery. *Curr. Opin. Ophthalmol.* **2012**, *23*, 269–275. [[CrossRef](#)]
34. Choi, S.R.; Kim, U.S. The correlation between angle kappa and ocular biometry in Koreans. *Korean J. Ophthalmol.* **2013**, *27*, 421–424. [[CrossRef](#)]
35. Gharaee, H.; Shafiee, M.; Hoseini, R.; Abrishami, M.; Abrishami, Y.; Abrishami, M. Angle Kappa Measurements: Normal Values in Healthy Iranian Population Obtained With the Orbscan II. *Iran. Red Crescent Med. J.* **2015**, *17*, e17873. [[CrossRef](#)]
36. Hashemi, H.; Khabazkhoob, M.; Yazdani, K.; Mehravaran, S.; Jafarzadehpur, E.; Fotouhi, A. Distribution of angle kappa measurements with Orbscan II in a population-based survey. *J. Refract. Surg.* **2010**, *26*, 966–971. [[CrossRef](#)]